1.E.1:2.G *Nuclear Physics* **60** (1964) 35—48;

THE REACTIONS Rh^{103}(p, d)Rh^{102} and Rh^{103}(p, t)Rh^{101} at 16.8 MeV

KIP S. THORNE † and EDWIN KASHY

Palmer Physical Laboratory, Princeton University ††

Received 26 May 1964

Abstract: The reactions Rh^{103}(p, d)Rh^{102} and Rh^{103}(p, t)Rh^{101} have been investigated using 16.8 MeV protons. The following Q values were measured: for Rh^{103}(p, d)Rh^{102} $Q = -7.144 \pm 0.016$ MeV; for Rh^{103}(p, t)Rh^{101} $Q = -8.275 \pm 0.017$ MeV. Excited levels of Rh^{101} were observed at 331, 869, 1041 and 1512 keV. The 331 keV level may be the 4.5 d isomer of Rh^{101}. Excited levels of Rh^{102} were observed at 76, 161, 291, 380, 491, 544, 680, 726, 1200, 1670 and 1840 keV. Angular distributions were measured for most of the levels; and, from the comparison of these distributions with distorted-wave Born approximation calculations and with each other, conclusions were drawn about the spin, parity and spectroscopic factors of some of the levels.

E NUCLEAR REACTIONS Rh^{103}(p, d), (p, t), $E_p = 16.8$ MeV; measured d-, t-spectra, Q, $\sigma(\theta)$. C^{13}(p, d), $E_p = 16.8$ MeV; measured $\sigma(\theta)$. $Rh^{101,102}$ deduced levels, J, π, l.

1. Introduction

Since naturally occurring rhodium is mono-isotopic, it has frequently been used as a representative element from its mass region in the investigation of nuclear properties via nuclear reactions. Elastic and inelastic scattering experiments [1]) have yielded much information about the level structure of Rh^{103}. However, because of the relatively close energy-level spacings in the rhodium isotopes and the negative Q values involved, little has been learned about Rh^{101} and Rh^{102} from the pickup reactions Rh^{103}(p, t)Rh^{101} and Rh^{103}(p, d)Rh^{102}. Blanpied and Sherr [2]) and Ball and Goodman [3]), who have investigated these reactions, did not have sufficiently good resolution to resolve individual levels. Consequently, our knowledge of Rh^{101} and Rh^{102} has been based mainly on the study of gamma ray spectra.

Recently it has been possible to obtain a proton beam with an energy spread of 25 keV from the Princeton University cyclotron. This, coupled with the powerful techniques provided by solid state detectors and two-dimensional analysers, motivated the re-investigation of pickup reactions in rhodium.

In discussing the level structure of rhodium, we shall use the spherical shell model, although the multiple configurations involved make detailed application questionable.

† Recipient of Woodrow Wilson National Fellowship and Danforth Foundation support for part of the period of this research.

†† This work was supported by the U.S. Atomic Energy Commission and the Higgins Scientific Trust Fund.

This model suggests that $_{45}Rh^{103}_{58}$ has eight neutrons in the major shell between magic numbers 50 and 82, which contains $1g_{\frac{7}{2}}$, $2d_{\frac{5}{2}}$, $1h_{\frac{11}{2}}$, $2d_{\frac{3}{2}}$ and $3s_{\frac{1}{2}}$ single-particle states; and five proton holes in the preceding major shell (magic numbers 50 to 28), which contains $1g_{\frac{9}{2}}$, $2p_{\frac{1}{2}}$, $1f_{\frac{5}{2}}$ and $2p_{\frac{3}{2}}$ states. The degree of configuration mixing among all these states may be very high. Some of the experimental results reported here, as well as the evidence for a deformed Rh^{103} nucleus in the form of the splitting of its giant dipole resonance [4]) are indications of a failure of the simple shell model.

2. Experimental Methods

Protons of 16.8 MeV energy were extracted from the Princeton FM cyclotron and steered and deflected through a magnetic analyser into a 50 cm scattering chamber. The proton beam was integrated using a Faraday cup. During much of the experiment the number of counts under the Rh^{103}(p, p)Rh^{103} elastic peak was monitored by a solid state detector. This served as a check on target deterioration and beam current integration.

The angular distributions and Q value measurements were taken with a 0.49 mg/cm^2 Rh^{103} target which was evaporated onto a 0.73 mg/cm^2 Mylar backing. The absolute normalization of the cross sections and the locations of peaks with very low yield were determined using a self-supporting 3.72 mg/cm^2 Rh^{103} foil of thickness uniform to within 2%.

The counter telescope used is described elsewhere [5]). Briefly, it consisted of a 50 μm ΔE detector, followed by a 500 μm E detector, followed by a third detector used to provide an anticoincidence gate. The energies of the deuterons and tritons were obtained by the coherent summing of the charges from the E and ΔE detectors.

A diagram of the detector circuitry and of the amplification and pulse-analysing systems is shown in fig. 1. A 1024 channel, two-dimensional analyser was used to measure the deuteron and triton spectra. In order to cut down pile-up events, the two dimensional analyser was blocked by a pulse from the third detector whenever an elastic or high-energy inelastic proton passed through the telescope. The same anticoincidence pulse blocked the monitor analyser as shown in fig. 1, and the rate of anticoincidence pulses was measured to provide a dead time correction to the integrated beam current. The thin target spectra obtained with this system showed peaks having full-widths-at-half maximum (FWHM) of 50 to 60 keV (cf. fig. 2).

The energy calibration procedure consisted of taking Rh^{103}(p, t)Rh^{101} and F^{19}(p, d)F^{18} or Ti^{49}(p, d)Ti^{48} data under similar conditions and comparing their spectra in the laboratory system. A 1 mg/cm^2 self-supporting Ti target enriched to 76% in Ti^{49}, and a 0.2 mg/cm^2 Teflon target were used in these measurements. The Teflon target was made by spraying Dupont Slip Spray, a Teflon suspension purchased from a local hardward store, onto 6.3 μm Mylar. In performing the calibration, the following Q values [6-9]) were assumed for the F and Ti reactions: F^{19}(p, d)F^{18} ground state -8.218, first excited level -9.158; Ti^{49}(p, d)Ti^{48} excited levels

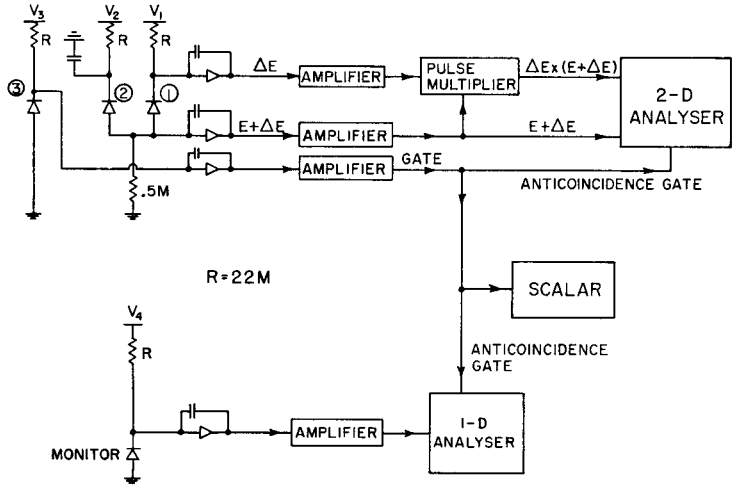

Fig. 1. Detector circuitry and pulse amplification and analysis systems.

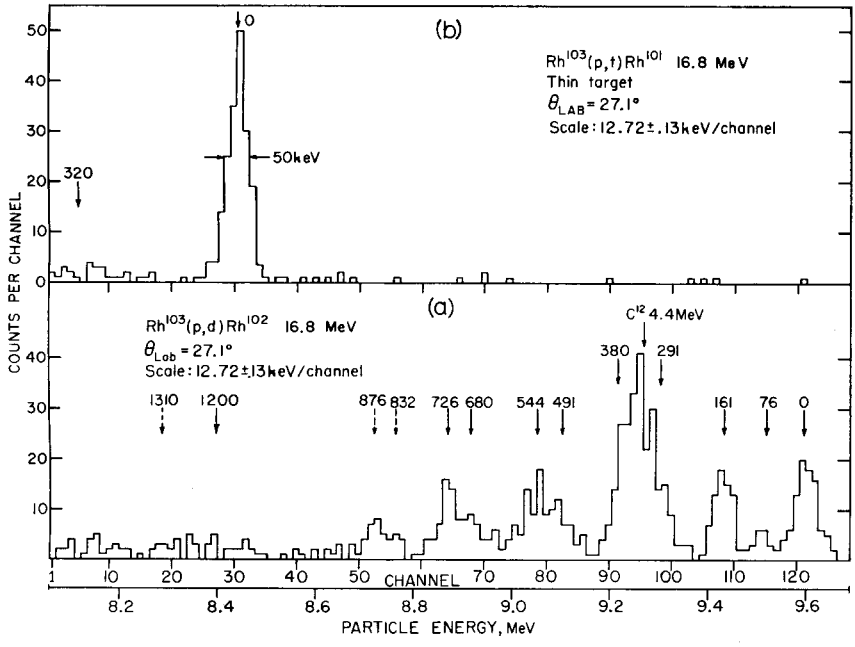

Fig. 2. Rh^{103}(p, d)Rh^{102} and Rh^{103}(p, t)Rh^{101} thin target spectra at 16.8 MeV. The positions of the identified energy levels, as determined by comparing all spectra taken, are indicated by arrows and labelled with their excitation energies. In (a) the C^{13}(p, d)C^{12*} impurity peak overlaps the 291 and 380 keV levels, but it shifts so rapidly with target angle that at 37.1° it overlaps the 544 keV level.

−6.900, −8.217, −9.152, −9.252, −9.425; Ti^{50}(p, d)Ti^{49} ground state −8.709; Ti^{48}(p, d)Ti^{47} first excited level −9.553.

An additional check on the Q values was provided, quite by accident, by the reaction C^{13}(p, d)C^{12*} going to the 4.4 MeV level of C^{12}. This reaction, resulting from the 1.1% abundance of C^{13} in the carbon of the Mylar backing of the rhodium target, produced a large peak, which shifted rapidly with detector angle, in the middle of the Rh^{103}(p, d)Rh^{102} spectrum.

The major sources of errors in the Q values and excited level energies are (i) uncertainty in peak positions due to finite peak widths and poor statistics (ii) uncertainty in target thicknesses and uniformity and in the rates of energy loss of particles in the targets, (iii) uncertainty in the Q values of the fluorine and titanium calibrating reactions. The major source of error in the absolute cross section calibration is statistical. The major sources of errors in the angular distributions are poor statistics and the problem of separating adjacent peaks from one another and from the C^{13}(p, d)C^{12*} peak.

3. Results and Discussion

3.1. DWBA CALCULATIONS

The angular distributions obtained for the levels excited in this experiment were compared with distorted wave Born approximation (DWBA) calculations to extract information about spins and parities. The DWBA calculations were performed using the Oak Ridge distorted wave code [10]) modified to include spin-orbit coupling. The proton optical parameters used were those which provide the best fit [11]) to the 17 MeV Rh^{103}(p, p)Rh^{103} elastic scattering data of Dayton and Schrank [12]). These parameters are listed in table 1.

TABLE 1

Optical well parameters used in analysis of the experimental data using the notation of Perey [11])

Particle	V_S	r_{oS}	$\frac{R_c}{A^{\frac{1}{3}}}$	a_S	W_D	W_S	r_{oI}	a_I	W_{so}	V_{so}
Proton	57.66	1.15	1.15	0.687	8.2	0	1.263	0.738	0	8.16
Deuteron	92.4	1.15	1.15	0.81	19.9	0	1.34	0.68	0	0
Triton	50	1.6	1.6	0.5	0	20	1.6	0	0	0

The (p, d) DWBA calculations used deuteron optical well parameters calculated by Perey and Perey [13]) to fit the 11.8 MeV Rh^{103}(d, d)Rh^{103} elastic scattering data of Igo *et al.* [14]) except that the real well depth was extrapolated to make it correspond to 9 MeV deuterons. Because of ambiguities in the deuteron elastic fits, Perey and Perey give four different sets of parameters (A, B, C, D) which fit the elastic scattering data equally well. Using the standard DWBA approach, angular distributions for the pickup of $2d_{\frac{3}{2}}$, $2d_{\frac{5}{2}}$ and $1g_{\frac{7}{2}}$ neutrons from Rh^{103} were calculated for all four sets of

deuteron optical parameters and were found to differ markedly from set to set. However, they were sufficiently similar to distinguish distributions for 2d neutrons from those for 1g neutrons. Of the four sets of parameters, set B gave the closest resemblance to the experimental deuteron pickup data. The parameters of this set, upon which all calculations discussed here were based, are given in table 1.

The neutron wave functions for the (p, d) calculations were computed using the real part of the proton optical well of table 1 with the well depth adjusted to give a neutron wave function having the proper binding energy.

A Rh^{103}(p, t)Rh^{101} DWBA calculation [15]) was performed using triton optical parameters given in table 1. The angular distribution was found to be fairly insensitive to the choice of these parameters. The (p, t) calculation used a model in which a dineutron, formed by coupling two 1g neutrons to zero angular momentum, was picked up. The radial part of the dineutron wave function was computed in a zero range approximation; it peaked at 6.0 fm and had a half width of 1.6 fm. The shape of the angular distribution was quite insensitive to the shape of the dineutron wave function.

3.2. THE Q VALUES AND ANGULAR DISTRIBUTIONS

The Rh^{103}(p, d)Rh^{102} and Rh^{103}(p, t)Rh^{101} thin target spectra were taken at 19 different angles ranging from 12 to 102 degrees. Protons of 16.8 MeV energy were used, and the energy region examined ran from the ground state of Rh^{102} to an excitation energy of 1.4 MeV. (See fig. 2 for sample spectra). The yields to levels of

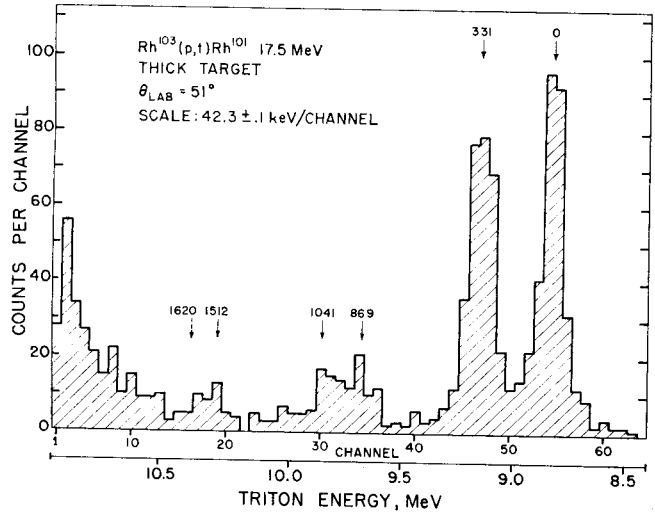

Fig. 3. Rh^{103}(p, t)Rh^{101} thick target spectrum at 17.5 MeV. The positions of the energy levels, as determined by comparing all spectra taken, are indicated by arrows and labelled with their excitation energies. This spectrum is taken at the second minimum in the angular distribution to the ground state of Rh^{101}.

Rh^{102} above 1 MeV and to all levels of Rh^{101} except its ground state were too low to permit use of the thin rhodium target. For this energy range spectra were taken with the thick target at 51°, 57° and 63° using 17.5 MeV protons. (See fig. 3 for a sample triton spectrum.) All spectra obtained were compared to locate and determine the energies of the levels listed in table 2 and shown in figs. 4 and 9.

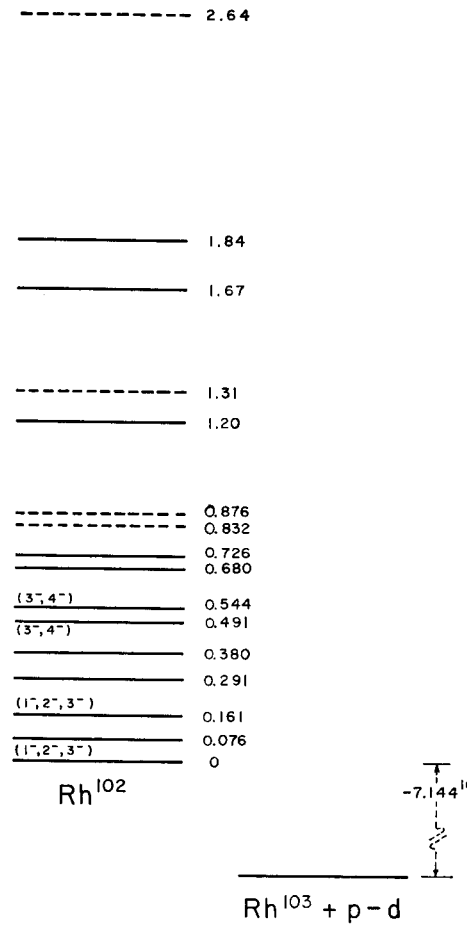

Fig. 4. Proposed energy level diagram for Rh^{102}.

The Q values calculated from the data are shown in table 3. Using these Q values and the mass [16]) of 102.905509±4 for Rh^{103}, one obtains for the masses of Rh^{101} and Rh^{102} on the C^{12} scale the values shown in table 4. The mass obtained for Rh^{102} is considerably higher than that calculated on other bases (cf. table 4). There are two possible explanations for this (i) The level which we have called the ground state of Rh^{102} might actually be its 2.5 y isomer, in which case the cross section for exciting the true ground state in the reaction Rh^{103}(p, d)Rh^{102} is less than 30 μb/sr. The spin

TABLE 2

Summary of level structures of Rh^{101} and Rh^{102} from the pickup reactions

Nucleus	Excitation energy (keV)	Picked-up neutrons	J^{π} [a]	$(\sigma_{cm})_{max}$ mb/sr	$(\theta_{cm})_{max}$ (degree)	Spectroscopic factor S
Rh^{101}	0	2 n's coupled to 0 spin	$\frac{1}{2}^-$	0.75	30	0.7
Rh^{101}	331±7 [b]			0.025 [c]		
Rh^{101}	869±9			0.004 [c]		
Rh^{101}	1041±10			0.003 [c]		
Rh^{101}	(1512±10)			0.004 [c]		
Rh^{101}	(1620±40)			$\lesssim$ 0.003 [c]		
Rh^{102}	0	2d	$(1^-, 2^-, 3^-)$	0.35	23	1.1 [d]
Rh^{102}	76±9			0.15	15	
Rh^{102}	161±6	2d	$(1^-, 2^-, 3^-)$	0.30	23	1.0 [d]
Rh^{102}	291±10			0.10	50	
Rh^{102}	380±7	(2d)		0.25	18	
Rh^{102}	491±9	$1g_{\frac{7}{2}}$	$(3^-, 4^-)$	0.17	28	9 [e]
Rh^{102}	544±9	$1g_{\frac{7}{2}}$	$(3^-, 4^-)$	0.25	30	12 [e]
Rh^{102}	680±13			0.15	40	
Rh^{102}	726±11	$(1g_{\frac{7}{2}})$		0.2	25	
Rh^{102}	(832±16)			0.07	32	
Rh^{102}	(876±17)			0.10	28	
Rh^{102}	1200±30			0.07 [c]		
Rh^{102}	(1310±20)			0.15	18	
Rh^{102}	1670±40			0.03 [c]		
Rh^{102}	1840±40			0.03 [c]		

[a]) Based on $J^{\pi} = \frac{1}{2}^-$ for Rh^{103}.
[b]) This level may be the 4.5 d isomer of Rh^{101}.
[c]) $(\sigma_{cm})_{max}$ was not measured. This is σ_{cm} at $\theta_{cm} = 55°$.
[d]) Based on $2d_{\frac{5}{2}}$ DWBA calculations.
[e]) Based on $1g_{\frac{7}{2}}$ DWBA calculations.

TABLE 3

Q values for the reactions Rh^{103}(p, d)Rh^{102} and Rh^{103}(p, t)Rh^{101} based upon fluorine, titanium and carbon energy calibrations

Calibration	Rh^{103}(p, d)Rh^{102}	Rh^{103}(p, t)Rh^{101}
F^{19}(p, d)F^{18}	−7.155±0.023	−8.285±0.017
Ti^{49}(p, d)Ti^{48}	−7.142±0.016	−8.264±0.018
C^{13}(p, d)C^{12}	−7.128±0.030	
Weighted average	−7.144±0.016	−8.275±0.017

See sect. 2 for description of calibration procedure.

of the level we have called the ground state is $(1^-, 2^-, 3^-)$, while the spin [19]) of the true ground state is $(0^-, 1^-, 2^-)$. Only a 0^- ground state and a 3^- isomer could be compatible with a 30 μb/sr Rh^{103}(p, d)Rh^{102} ground state cross section and with an isomer half life of 2.5 y and excitation energy of $\approx$ 60 keV. (ii) There may be a systematic error in one or more of the experiments. The mutual incompatibility of the masses based on the β-decay experiments make them possible culprits. If the β-decay masses are discarded, the remaining $Rh^{103}(\gamma, n)Rh^{102}$ mass is statistically compatible with our mass.

TABLE 4

Masses of Rh^{101} and Rh^{102} on the C^{12} scale

Basis of value	Ref.	Mass of Rh^{101}	Mass of Rh^{102}
Pick-up reactions	Present work	100.906 168±18	101.906 901±17
$Rh^{102}(\beta^+)Ru^{102}$	[17])		101.906 812±13
$Rh^{102}(\beta^-)Pd^{102}$	[17])		101.906 859±20
$Rh^{103}(\gamma, n)Rh^{102}$	[18])		101.906 836±34

The values calculated from the present reaction studies are compared with values calculated [5]) on other bases.

The angular distributions obtained with the thin target for Rh^{103}(p, d)Rh^{102} are shown in figs. 5–7, where they are compared with DWBA calculations. From the resemblance of the ground state, the 161 keV and possibly the 380 keV angular distributions to each other to $l = 2$ DWBA calculations and to $l = 2$ angular distributions in the $A = 90$ mass region [20]), we conclude that the angular distributions of fig. 5 are $l = 2$. The 491, the 544 and possibly the 726 keV angular distributions (fig. 6) are probably due to $1g_{\frac{7}{2}}$ pickup, since these angular distributions are markedly similar and $1g_{\frac{7}{2}}$ is the only DWBA calculation which resembles them. Some of the angular distributions in figs. 5 and 6 (in particular, those for the 380 and 720 keV levels) may be mixtures of $l = 2$ and $l = 4$. The 680 keV angular distribution (fig. 7) resembles a $1f_{\frac{5}{2}}$ DWBA calculation, but poor statistics and the shell model make this association questionable. From these l assignments we obtain the spins and parities listed in table 2. Note that the agreement between the experimental angular distributions and the DWBA calculations is not good. This may be caused by the non-sphericity of the Rh^{103} nucleus [4]).

The angular distribution for (p, t) pickup to the ground state of Rh^{101} (fig. 8) is well described by a DWBA calculation for the pickup of two 1g neutrons coupled to zero angular momentum and positive parity. This beautiful $l = 0$ angular distribution, together with the large cross section for this reaction (larger, in fact, than that for the (p, d) reaction to any two levels of Rh^{102} and twenty times larger than the (p, t) cross section to any other level of Rh^{101}), makes it quite certain that the spin of Rh^{101}, like that of Rh^{103}, is $\frac{1}{2}^-$.

3.3. THE LEVEL STRUCTURE AND THE 4.5 d ISOMER OF Rh^{101}

Until now our knowledge of the level structure of Rh^{101} has come solely from the γ-decay study of Pd^{101} by Katcoff and Abrash [21]) and from the observation of a 158 keV internal conversion transition in the decay of Rh^{101} by Farmer [22]) and by

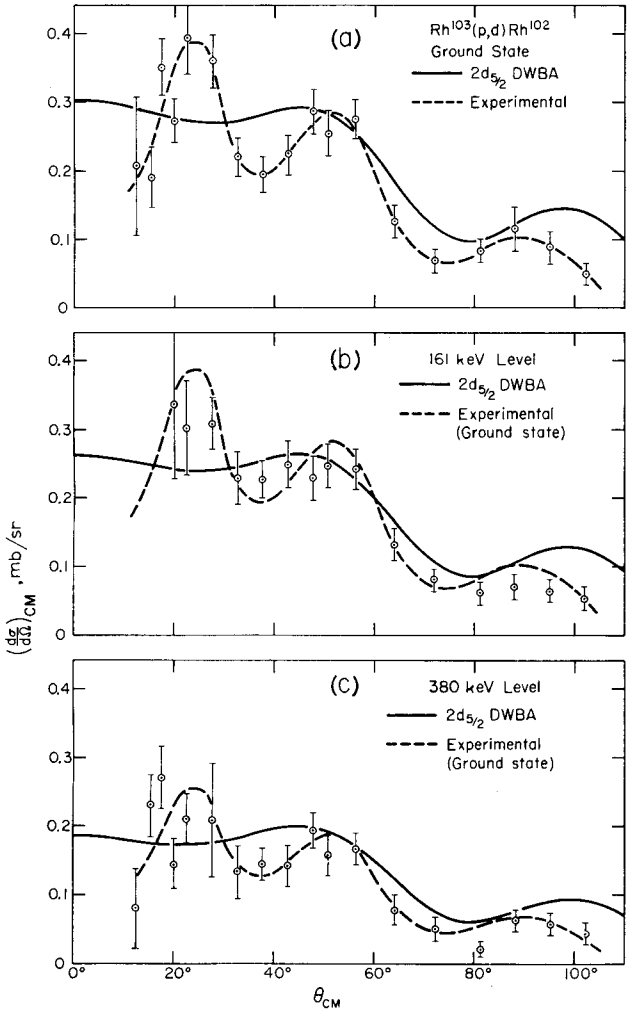

Fig. 5. The $l = 2$ angular distributions for the reaction $Rh^{103}(p, d)Rh^{102}$. There is an uncertainty of ± 10 % in the absolute cross section calibration of the data. DWBA calculations for $2d_{\frac{3}{2}}$ pickup are shown for comparison. The $2d_{\frac{3}{2}}$ calculations were very similar to the $2d_{\frac{5}{2}}$ calculations.

Fultz *et al.* [23]). On these bases the Nuclear Data Group [24]) has suggested the level scheme shown in fig. 9(a). This scheme is not in agreement with the level structure found in the present investigation (table 2). We suggest that in view of all experimental evidence now available, fig. 9(b) is the most reasonable level scheme for Rh^{101}.

To obtain scheme (b) we must postulate the existence of a 600 keV level in Rh^{101}, which we do not see in the reaction $Rh^{103}(p, t)Rh^{101}$, and which therefore has a cross section less than 1 μb/sr at laboratory angles between 51° and 57°. Scheme (b)

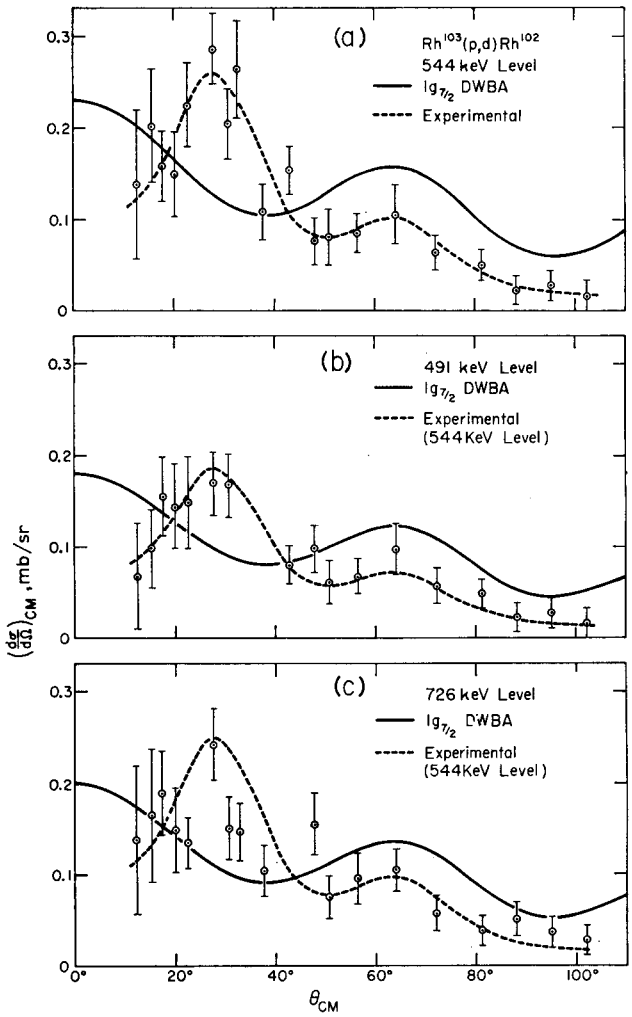

Fig. 6. The $l = 4$ angular distributions for the reaction $Rh^{103}(p, d)Rh^{102}$. These distributions are distinguished from the $l = 2$ distributions (fig. 5) primarily by their behaviour in the region between 40° and 60°. There is an uncertainty of $\pm 10\,\%$ in the absolute cross section calibration of the data. The DWBA calculations for $1g_{\frac{7}{2}}$ pickup are shown for comparison; $1g_{\frac{9}{2}}$ calculations were quite different from the $1g_{\frac{7}{2}}$ calculations.

also requires that the 4.5 d isomer of Rh^{101} have an excitation energy of 331 keV rather than 158 keV. If this is correct, then the 158 keV internal conversion transition seen by Farmer [22]) and by Fultz *et al.* [23]) is unaccounted for. The evidence in the

literature for the association of the observed conversion electrons with a 158 keV transition in Rh^{101} is not particularly strong, but Farmer[26]) reports that unpublished

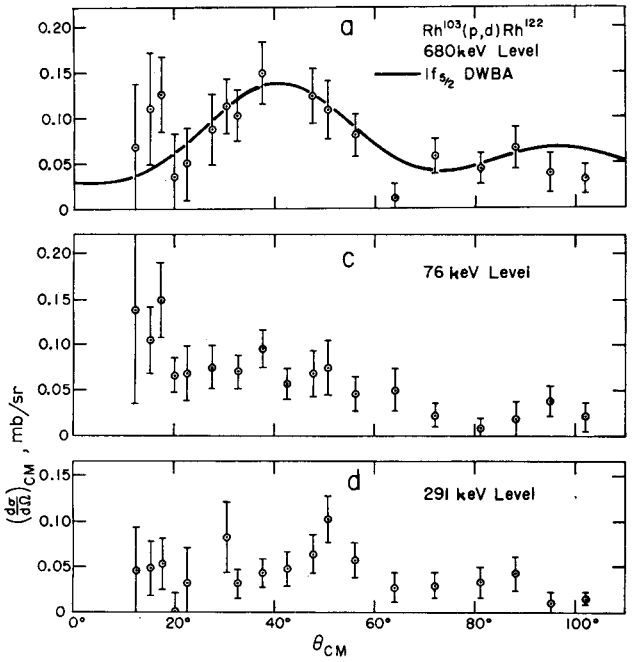

Fig. 7. Angular distributions of uncertain l value for the reaction Rh^{103}(p, d)Rh^{102}. There is an uncertainty of $\pm 10\,\%$ in the absolute cross section calibration of the data.

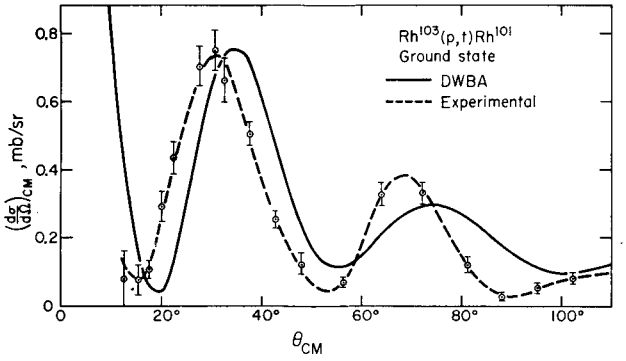

Fig. 8. Angular distribution for the reaction Rh^{103}(p, t)Rh^{101} going to the ground state of Rh^{101}. There is an uncertainty of $\pm 10\,\%$ in the absolute cross section calibration of the data.

aspects of his own work convince him of the validity of the association. If, indeed, a 158 keV level exists in Rh^{101} the cross section for exciting it in the reaction Rh^{103}(p, t)Rh^{101} at a laboratory angle of 51° is less than 4 μb/sr. If scheme (b) is

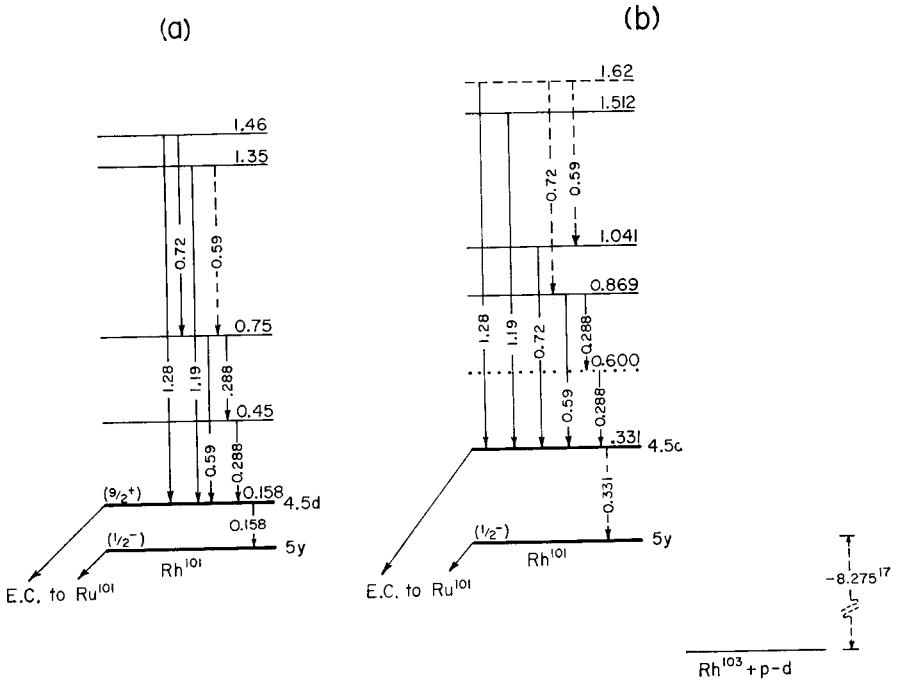

Fig. 9. The level scheme for Rh^{101} (a) suggested by the Nuclear Data Group [24]) on the basis of γ-decay studies, (b) in greatest agreement with the present nuclear reaction investigation and previous γ-decay studies. The 600 keV level is *not* seen in our work.

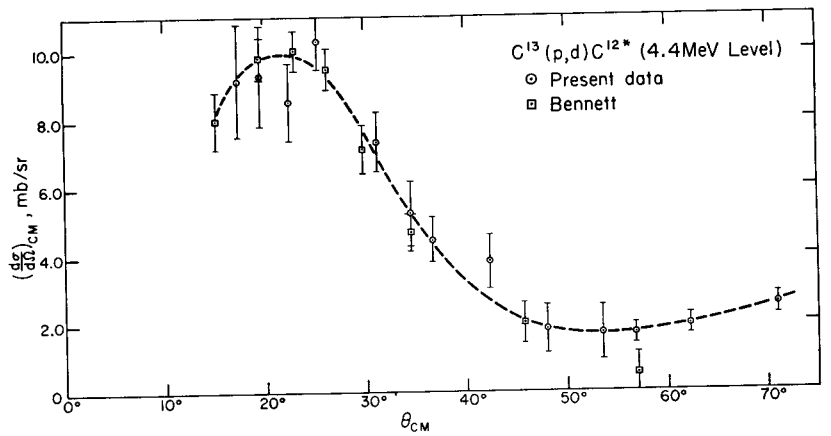

Fig. 10. The C^{13}(p, d)C^{12*} reaction going to the 4.4 MeV state of C^{12}. There is an uncertainty in the cross section calibration of $\pm 20\%$. Both data obtained in this investigation with 16.8 MeV protons and those of Bennett [25]) with 17.0 MeV protons are shown. The dotted line was empirically drawn through the data.

correct, then the conversion electrons and γ-rays from the 4.5 d 331 keV transition may be hidden among those from the 310 keV transition in the daughter nucleus Ru^{101}.

Note added in proof: Prelimary results of a recent investigation of Pd^{101} decay [27]) confirm the existence of a 158 keV isometric transition in Rh^{101}.

3.4. THE $C^{13}(p, d)C^{12*}$ REACTION

As mentioned in sect. 2, the reaction $C^{13}(p, d)C^{12*}$ going to the 4.4 MeV level of C^{12} was observed as a contaminant due to the C^{13} in the target backing. A side product of the experiment was the angular distribution for this reaction shown in fig. 10. The distribution agrees well with the data of Bennett [25]), which are also shown in fig. 10, and provides an absolute cross section calibration for the data. The C^{13} target thickness used in obtaining the cross section calibration was calculated from a knowledge of the thickness of the Mylar backing of the rhodium target, the fraction (by weight) of Mylar which is carbon, and the natural isotopic abundance of C^{13}.

The authors wish to thank Professor Rubby Sherr for suggesting this problem and for valuable advice and discussions through out its execution. They also wish to express appreciation to Professor B. Bayman and Dr. E. Rost for helpful discussions of the theoretical interpretation of the data. Dr. Rost also provided valuable advice and assistance with the DWBA calculations. The calculations were performed on the Princeton University IBM 7090 computer which was made possible by National Science Foundation Grant NSF-GP579.

References

1) B. L. Cohen and A. G. Rubin, Phys. Rev. **11** (1958) 1568;
B. L. Cohen and R. E. Price, Phys. Rev. **23** (1961) 282;
M. Crut, D. R. Sweetman and N. S. Wall, Nuclear Physics **17** (1960) 655
2) W. Blanpied and R. Sherr, Bull. Am. Phys. Soc. **2** (1957) 303
3) J. B. Ball and C. D. Goodman, Phys. Rev. **118** (1960) 1062, **120** (1960) 488
4) O. V. Bogdankevich, B. I. Goryachev and V. A. Zapevalov, JETP **42** (1962) 1502, JETP (Soviet Physics) **15** (1962) 1044
5) E. Kashy, Phys. Rev. **134** (1964) B378
6) T. Lauritsen and F. Ajzenberg-Selove, Energy levels of light nuclei, May, 1962 (National Academy of Sciences-National Research Council, Washington, 1962)
7) O. Hansen, Nuclear Physics **28** (1961) 140
8) E. Kashy and T. W. Conlon, Phys. Rev. **135** (1964) B389
9) UCRL Report No. 5419, unpublished
10) R. H. Bassel, R. N. Drisko and G. R. Satchler, Oak Ridge National Laboratory Report No. 3240, unpublished
11) F. G. Perey, Phys. Rev. **131** (1963) 745
12) I. E. Dayton and G. Schrank, Phys. Rev. **101** (1956) 1358
13) C. M. Perey and F. G. Perey, Phys. Rev. **132** (1963) 755
14) G. Igo, W. Lorenz and U. Schmidt-Rohr, Phys. Rev. **124** (1961) 832
15) E. Rost, private communication
16) R. A. Damerow, R. R. Ries and W. H. Johnson, Phys. Rev. **132** (1963) 1673

17) Nuclear Data Sheet NRC 61-2-42
18) K. N. Geller, J. Halpern and G. Muirhead, Phys. Rev. **118** (1960) 1302
19) Nuclear Data Sheet NRC 61-2-38
20) R. H. Bassel, R. N. Drisko and G. R. Satchler, in Direct interactions and nuclear reaction mechanisms, ed. by E. Clementel and C. Villi (Gordon and Breach, New York, 1963)
21) S. Katcoff and H. Abrash, Phys. Rev. **99** (1956) 10
22) D. J. Farmer, Phys. Rev. **99** (1955) 659A
23) S. C. Fultz, R. J. Nash, R. L. Woodward and M. L. Pool, Phys. Rev. **88** (1952) 170A; C. L. Scoville, S. C. Fultz and M. L. Pool, Phys. Rev. **85** (1952) 1046
24) Nuclear Data Sheet NRC 61-2-26
25) E. F. Bennett, Phys. Rev. **122** (1961) 595
26) D. J. Farmer, private communication
27) J. S. Evans, E. Kashy R. A. Naumann and R. F. Petry, private commucation